An Artificial Compressibility Method for the Spectral Difference Solution of Unsteady Incompressible Navier-Stokes Equations on Multiple Grids

Chunlei Liang [*], Andre Chan [†], Xiang Liu [‡], Antony Jameson [§]

This paper presents the development of a 2D high-order solver with unstructured spectral difference method for unsteady incompressible Navier-Stokes equations. Time-marching methods cannot be applied directly to incompressible flows because the governing equations are not hyperbolic. An artificial compressibility method (ACM) is employed in order to treat the inviscid fluxes using the traditional characteristics-based schemes. The viscous fluxes are computed using the averaging approach.[10,25] A dual time stepping scheme is implemented to deal with physical time marching. A p-multigrid method is implemented[14] in conjunction with the dual time stepping method for convergence acceleration. The SD method added with the ACM (SD-ACM) is able to accurately simulate 2D incompressible steady and unsteady viscous flows.

I. Introduction

In order to assist the design of devices which generate vortex dominated flows, such as micro air vehicle, wind turbine and tidal turbine blades, high-order unstructured methods become attractive due to its outstanding ability to control numerical dissipation. The aforementioned vortex dominated flows are largely incompressible and highly viscous and unsteady. In this paper, the development of an incompressible spectral difference (ISD) method for solving unsteady viscous flows is reported.

The Spectral Difference (SD) Method is a high-order efficient high-order approach based on differential strong form of the governing equations. The SD method combines elements from finite-volume and finite-difference techniques. It is able to achieve optimal order of accuracy for various compressible flows.[10,12,13,25] The method is particularly attractive because it is conservative, and has a simple formulation and easy to implement. The first papers of unstructured SD method[16,29] were developed for wave equations and compressible Euler equations respectively. Recently, it has been further developed for solving 3D turbulent compressible flows.[3,15,19,20]

One of the many challenges in solving incompressible Navier-Stokes equations comes from the weak coupling of the velocity and pressure fields. This coupling has to be treated in such a way as to ensure divergence-free of velocities. Two group of commonly used methods for handling velocity-pressure coupling in incompressible flows are pressure correction approach and artificial compressibility method.

The pressure-correction method (PCM) is perhaps the mostly widely used for incompressible flows. It was introduced by Harlow and Welch[8] for the calculation of unsteady flows. The basic idea is to formulate a Poisson equation for pressure corrections, and then to update the pressure and velocity fields until a divergence-free velocity field is reached.

The artificial compressibility method (ACM) for calculating steady flows was proposed by Chorin.[4] In this method, an artificial compressibility term is added to the continuity equation, and the unsteady terms in the momentum equations are returned. Hence, without considering the viscous terms, the system of equations becomes hyperbolic and traditional techniques developed for solving subsonic compressible flows can be applied. For unsteady flow problems, a dual time stepping scheme can be used together the ACM.

[*]Assistant professor,George Washington University, AIAA Senior Member.
[†]PhD student, Stanford University, AIAA Senior Member.
[‡]Nexant Inc, San Francisco.
[§]Professor, Stanford University, AIAA Fellow.

Rosenfeld et al[22] extended the ACM method to solve unsteady problems. To accelerate solution convergence within each physical time step, a multigrid method can be employed. Farmer et al[6] developed a multigrid scheme for the solution of the Euler equations in conjunction with the ACM and applied it to free surface flows. Yuan[31] implemented a geometric multigrid method for the ACM and successfully solved steady and unsteady viscous flow. Bassi et al.[2] firstly proposed an exact Riemann flux for ACM and successfully extended the discontinuous Galerkin method to handle steady incompressible flow problems.

The remaining part of this paper is arranged as the following. Section II provides the numerical formulation of the SD method. Section III presents the ACM formulations. In section IV, the approach to implementation of a p-multigrid method is reported. In section V, verification study of Taylor Couette flow is reported. Section VI presents simulations of laminar flow past a circular cylinder at Reynolds numbers 20 and 185 respectively.

II. Numerical Formulation of the SD method

The formulations of the equations employed in this paper are largely similar to the formulations of Liang et al[12] for unstructured quadrilateral grids. Consider the unsteady incompressible 2D Navier Stokes equations in conservative form

$$\frac{\partial Q}{\partial t} + \frac{\partial F}{\partial x} + \frac{\partial G}{\partial y} = 0 \tag{1}$$

where Q is the vector of conserved variables; F and G are the total fluxes including both inviscid and viscous flux vectors, i.e. $\nabla \mathbf{F}_I - \nabla \mathbf{F}_V = \frac{\partial F}{\partial x} + \frac{\partial G}{\partial y}$. To achieve an efficient implementation, all elements in the physical domain (x, y) are transformed into a standard square element ($0 \leq \xi \leq 1$ and $0 \leq \eta \leq 1$).

The transformation can be written as:

$$\begin{pmatrix} x \\ y \end{pmatrix} = \sum_{i=1}^{K} M_i(\xi, \eta) \begin{pmatrix} x_i \\ y_i \end{pmatrix} \tag{2}$$

where K is the number of points used to define the physical element, (x_i, y_i) are the cartesian coordinates at those points, and $M_i(\xi, \eta)$ are the shape functions. For present implementation, we define K as 4 nodal points for a linear element and 8 nodal points for a quadratic element. The metrics and the Jacobian of the transformation can be computed for each element. The Jacobian is can be expressed as:

$$J = \begin{pmatrix} x_\xi & x_\eta \\ y_\xi & y_\eta \end{pmatrix} \tag{3}$$

The governing equations in the physical domain are then transferred into the computational domain, and the transformed equations take the following form:

$$\frac{\partial \tilde{Q}}{\partial t} + \frac{\partial \tilde{F}}{\partial \xi} + \frac{\partial \tilde{G}}{\partial \eta} = 0 \tag{4}$$

where $\tilde{Q} = |J| \cdot Q$ and

$$\begin{pmatrix} \tilde{F} \\ \tilde{G} \end{pmatrix} = |J| J^{-1} \begin{pmatrix} F \\ G \end{pmatrix} \tag{5}$$

In the standard element, two sets of points are defined, namely the solution points and the flux points, which are illustrated in figure 1.

In order to construct a degree $(N-1)$ polynomial in each coordinate direction, solution at N points are required. The solution points in 1D are chosen to be the Gauss points defined by:

$$X_s = \frac{1}{2}\left[1 - cos\left(\frac{2s-1}{2N} \cdot \pi\right)\right], s = 1, 2, \cdots, N. \tag{6}$$

The flux points were chosen as Legendre-Gauss quadrature points plus the two end points 0 and 1, as suggested by[9] and.[28] Choosing $P_{-1}(\xi) = 0$ and $P_0(\xi) = 1$, we can determine the higher-degree Legendre polynomials as

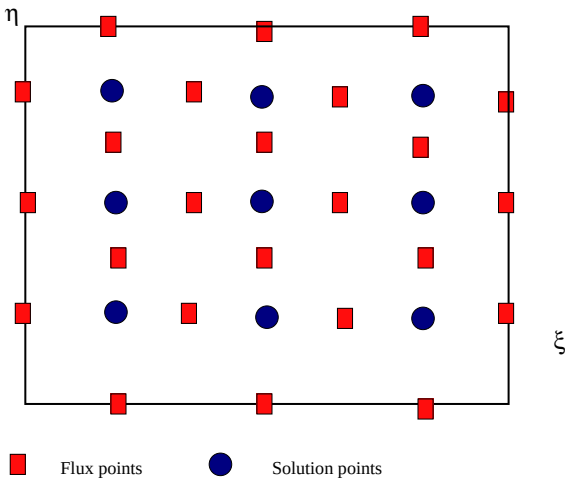

Figure 1. Distribution of flux and solution points for the third order SD scheme

$$P_n(\xi) = \frac{2n-1}{n}(2\xi - 1)P_{n-1}(\xi) - \frac{n-1}{n}P_{n-2}(\xi) \tag{7}$$

The locations of these Legendre-Gauss quadrature points are the roots of equation $P_n(\xi) = 0$.

Using the solutions at N solution points, a degree $(N-1)$ polynomial can be built using the following Lagrange basis defined as:

$$h_i(X) = \prod_{s=1, s\neq i}^{N} \left(\frac{X - X_s}{X_i - X_s} \right) \tag{8}$$

Similarly, using the fluxes at $(N+1)$ flux points, a degree N polynomial can be built for the flux using a similar Lagrange basis defined as:

$$l_{i+1/2}(X) = \prod_{s=0, s\neq i}^{N} \left(\frac{X - X_{s+1/2}}{X_{i+1/2} - X_{s+1/2}} \right) \tag{9}$$

The reconstructed solution for the conserved variables in the standard element is just the tensor products of the three one-dimensional polynomials,

$$Q(\xi, \eta) = \sum_{j=1}^{N} \sum_{i=1}^{N} \frac{\tilde{Q}_{i,j}}{|J_{i,j}|} h_i(\xi) \cdot h_j(\eta) \tag{10}$$

Similarly, the reconstructed flux polynomials take the following form:

$$\begin{aligned} \tilde{F}(\xi, \eta) &= \sum_{j=1}^{N} \sum_{i=0}^{N} \tilde{F}_{i+1/2,j} l_{i+1/2}(\xi) \cdot h_j(\eta), \\ \tilde{G}(\xi, \eta) &= \sum_{j=0}^{N} \sum_{i=1}^{N} \tilde{G}_{i,j+1/2} h_i(\xi) \cdot l_{j+1/2}(\eta) \end{aligned} \tag{11}$$

The reconstructed fluxes are only element-wise continuous, but discontinuous across cell interfaces. In our case, we have used the simple Rusanov solver[23] to compute the interface inviscid fluxes. An averaging approach[10,25] is employed for computing viscous fluxes at these interfaces.

In summary, the algorithm to compute the inviscid flux derivatives consists of the following steps:

1. Given the conservative variables at the solution points, the conservative variables are computed at the flux points. The inviscid fluxes at the interior flux points can also be determined from the polynomials based on the solution points.

2. The inviscid fluxes at the element interfaces are computed using the Riemann solver. Given the normal direction of the interface n, and the averaged normal velocity component V_n and the sound speed c, the inviscid flux on the interface can be determined.

3. The derivatives of the inviscid fluxes are computed at the solution points using the derivatives of Lagrange operators l

$$\begin{aligned}\left(\frac{\partial \tilde{F}}{\partial \xi}\right)_{i,j} &= \sum_{r=0}^{N} \tilde{F}_{r+1/2,j} \cdot l'_{r+1/2}(\xi_i), \\ \left(\frac{\partial \tilde{G}}{\partial \eta}\right)_{i,j} &= \sum_{r=0}^{N} \tilde{G}_{i,r+1/2} \cdot l'_{r+1/2}(\eta_j)\end{aligned} \tag{12}$$

4. The convective term $\nabla \mathbf{F}_I(Q)$ can be readily determined after transforming these derivatives back the physical domain.

III. Formulation of the Artificial Compressibility Method

The 2D Navier-Stokes equations have an additional viscous terms dependent on not only conservative variables but also their gradients. To illustrate the treatment of viscous flow terms, one can write the Navier-Stokes equations in conservation terms as

$$\frac{\partial Q}{\partial t} + \nabla \mathbf{F}_I(Q) - \nabla \mathbf{F}_V(Q, \nabla Q) = 0 \tag{13}$$

The conservative variables Q and Cartesian components $f_I(Q)$ and $g_I(Q)$ of the inviscid flux vector $\mathbf{F}_I(Q)$ are given by

$$Q = \begin{Bmatrix} p \\ u \\ v \end{Bmatrix}, \quad f_I(Q) = \begin{Bmatrix} \gamma u \\ u^2 + p \\ uv \end{Bmatrix}, \quad g_I(Q) = \begin{Bmatrix} \gamma v \\ uv \\ v^2 + p \end{Bmatrix} \tag{14}$$

Here ρ is the density, u and v are the velocity components in x and y directions, $p = P/\rho$ and P stands for the static pressure. The ratio γ is chosen as 1.25.

We define the element interface normal velocity as $V_n = un_x + vn_y$ and $c = \sqrt{V_n^2 + \gamma}$. Three characteristics for the above incompressible flow system with artificial compressibility are $V_n + c$, V_n and $V_n - c$.

The Cartesian components $f_V(Q, \nabla Q)$ and $g_V(Q, \nabla Q)$ of viscous flux vector $\mathbf{F}_V(Q, \nabla Q)$ are given by

$$\begin{aligned} f_V(Q, \nabla Q) &= \begin{Bmatrix} 0 \\ \nu u_x \\ \nu v_x \end{Bmatrix}, \\ g_V(Q, \nabla Q) &= \begin{Bmatrix} 0 \\ \nu u_y \\ \nu v_y \end{Bmatrix} \end{aligned} \tag{15}$$

where ν is the kinematic viscosity.

The procedures to get viscous fluxes can be described as the following steps:

1. reconstruct Q_f at the flux points from the conservative variables at the solution points using equation (10).

2. average the field of Q_f on the element interfaces as $\overline{Q_f} = \frac{1}{2}(Q_f^L + Q_f^R)$. For interior flux points, $\overline{Q_f} = Q_f$. Meanwhile, appropriate boundary conditions shall be applied for specific edge flux points.

3. evaluate ∇Q at solution points from $\overline{Q_f}$ using equation (12) where $\nabla Q = \left\{ \begin{array}{c} Q_x \\ Q_y \end{array} \right\}$ and $Q_x = \frac{\partial Q}{\partial \xi}\xi_x + \frac{\partial Q}{\partial \eta}\eta_x$, etc.

4. reconstruct ∇Q from solution points to flux points and using equation (10), average them on the element interfaces as $\overline{\nabla Q_f} = \frac{1}{2}(\nabla Q_f^L + \nabla Q_f^R)$

5. use $\overline{Q_f}$ and $\overline{\nabla Q_f}$ in order to compute the viscous flux vectors described in equation (15) at the element interfaces.

III.A. Time marching scheme

We write Eq. (13) in a different form by adding a pseudo-time derivative term:

$$\partial Q/\partial \tau + R^*(Q) = 0 \tag{16}$$

where $R^*(Q) = \partial Q/\partial t + \nabla \mathbf{F}_I(Q) - \nabla \mathbf{F}_V(Q, \nabla Q)$.

Flows with either steady or unsteady solutions are considered in this paper. All computations utilize a fourth-order accurate, strong-stability-preserving five-stage Runge-Kutta scheme[24] for treating the pseudo time τ and a second-order backward Euler scheme to deal with the physical time marching, i.e. $\partial Q/\partial t \approx \frac{1}{2\Delta t}\left(3Q^* - 4Q^n + Q^{n-1}\right)$. For the continuity equation, $\partial Q/\partial t$ is set as zero.

IV. p-multigrid Method

The p-multigrid method has been implemented in conjunction with the spectral difference method for compressible Euler equations[14] and compressible Navier-Stokes equations.[21]

Firstly, we try to solve $R_p^*(Q_p) = r_p$, $r_p = 0$ for the highest polynomial level p. A recursive V cycle routine ($V\_cycle(p)$) is implemented which consists of the following steps:

- Iterate over pseudo time step at level p for smoothing according to Eq. (16).
- Compute the defect at level p by

$$d_p = r_p - R_p^*(Q_p) = -R_p^*(Q_p) \tag{17}$$

- Restrict the latest solution and the defect to the lower polynomial level $p-1$ by

$$Q_{p-1}^0 = I_p^{p-1}(Q_p) \tag{18}$$

$$d_{p-1} = I_p^{p-1} d_p \tag{19}$$

- call the recursive subroutine at lower level as $V\_cycle(p-1)$
- prolongate the correction $Q_{p-1} - Q_{p-1}^0$ as

$$C_p = I_{p-1}^p(Q_{p-1} - Q_{p-1}^0) \tag{20}$$

- correct the solution at p level using $\tilde{Q}_p = Q_p + C_p$.
- Iterate over pseudo time step at level p for smoothing according to Eq. (16).

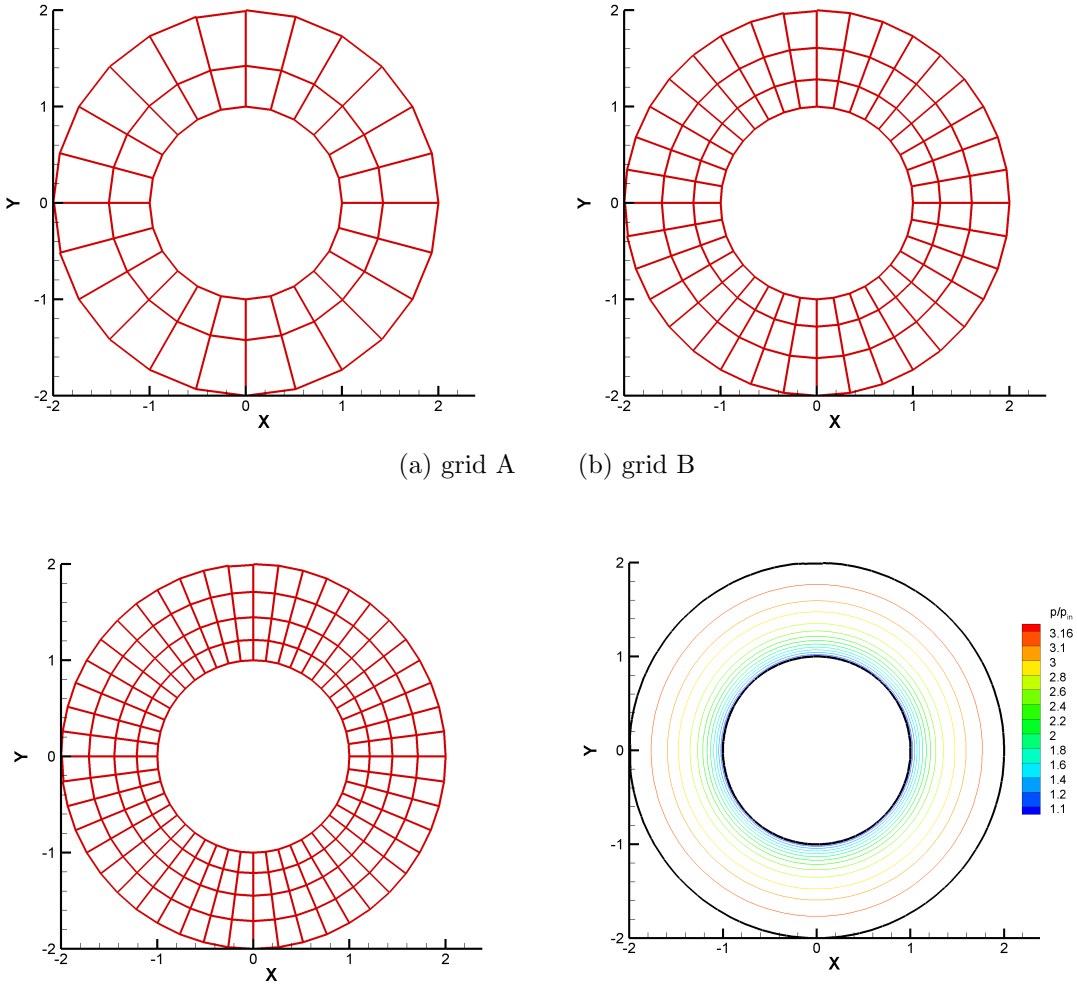

(a) grid A (b) grid B

(c) grid C (d) Pressure on grid B and ISD-4

Figure 2. Meshes for Incompressible Taylor Couette Flow

V. Verification study

In this example, the numerical order of accuracy is validated against the analytical solution for the incompressible Taylor Couette flow. This test problem was often referred to the original work by G. I. Taylor.[26] Recently, it was simulated by Michalak and Ollivier-Gooch[18] and Liang et al[11] for compressible flow. The exact solutions of angular velocity for both compressible flow and incompressible flow are identical. The angular velocity can be expressed as $V(r) = r_i\omega_i \frac{r_o/r - r/r_o}{r_o/r_i - r_i/r_o} + r_o\omega_o \frac{r/r_i - r_i/r}{r_o/r_i - r_i/r_o}$, where r_i and r_o stand for the radius of inner and outer cylinders respectively, and ω_i and ω_o refer to angular speed of inner and outer cylinders respectively.

A cubic curved wall boundary is used for both inner and outer cylinders. The inner cylinder spins clockwisely at a speed of 10 and the outer cylinder is fixed. No-slip boundary conditions are applied for both inner and outer cylinders. The Reynolds number is 10 based on inner cylinder spinning tangential velocity, its radius (=1) and $\nu = 1$. Three grids with 24×2, 36×3 and 48×4 cells are shown in figure 2. Fig. 2 (d) presents a typical pressure contour obtained by the fourth-order ISD method for the incompressible Taylor-Couette flow.

We obtained desired numerical orders in terms of $L1$ and $L2$ accuracies for V velocity component as shown in table 1. The results shown in table 1 are obtained using three levels of polynomails for both third-order and four-order ISD method. For the multigrid method with the highest p level of 3, a V cycle consists of 1-1-6-1-1 iterations at $p = 3$, $p = 2$ and $p = 1$ respectively. On the other hand, for the multigrid method with the highest p level of 4, a V cycle consists of 1-1-6-1-1 iterations at $p = 4$, $p = 2$ and $p = 1$ respectively. The maximum accuracy of fourth-order is demonstrated in the table. The explicit Runge-Kutta scheme becomes slow when the polynomial order is increased. However, the fifth-order and even higher accuracy can also be demonstrated using the implicit LU-SGS method.[14]

Figures 3 (a) and (b) present the U-compenent and V-component velocity contours respectively. These computations were performed on grid B using the fourth-order ISD method with the aforementioned three-level p-multigrid method.

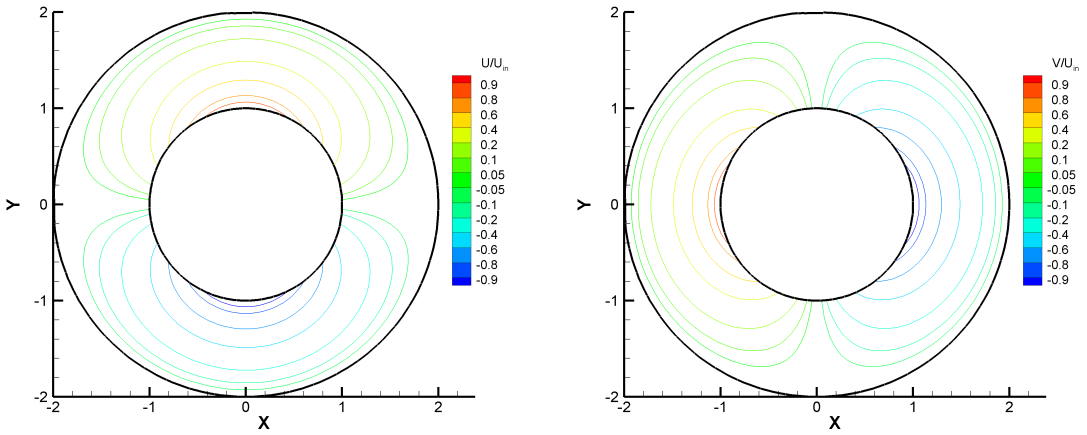

(a) U contour (b) V contour

Figure 3. U and V velocity contours obtained for incompressible Taylor Couette flow. The computations were performed on grid B and using the fourth-order ISD method.

Figures 4 (a) and (b) present the residual dropping rates against physical time and CPU time respectively. The computations on a single-level grid were performed on grid B using the fourth-order ISD method. In contrast, the computations on a three-level p-multigrid were performed using V cycles consisting of 1-1-6-1-1 iterations of smoothing operations on $p = 4$, $p = 2$ and $p = 1$ respectively. Both single-level and three-level computations were performed at the same time step size $\Delta t = 8 \cdot 10^{-4}$ for marching over physical time using the second-order backward differencing scheme and $\Delta\tau = 4 \cdot 10^{-4}$ for marching over pseudo time using the RK5 scheme. The three-level p-multigrid method requires less than half of the physical time to drop the residual level below $3 \cdot 10^{-11}$ compared to the single-level fourth order ISD method. From figure 4 (b), one can see that a speedup factor of approximately four is obtained by the three-level p-multigrid method.

This test case verifies that the 2D code remains its ability to generate optimal order of accuracy even

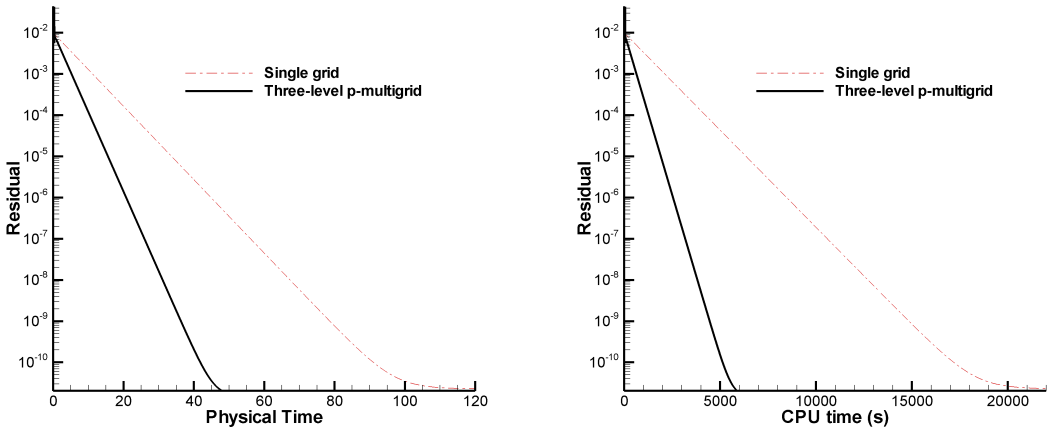

(a) Residual against physical time t (b) Residual against CPU time

Figure 4. Residual dropping rates against physical time and CPU time obtained by the four-order ISD method on single-p and three-p levels.

No. of elements	No. of DOFs	L2-error	Order	L1-error	Order
3rd order SD					
24×2	432	8.09E-3	-	6.968E-3	-
36×3	972	2.827E-3	2.6	2.432E-3	2.6
48×4	1728	9.817E-4	3.1	8.116E-4	3.04
96×8	6912	1.623E-4	2.6	1.256E-4	2.69
4th order SD					
24×2	768	1.994E-3	-	1.768E-3	-
36×3	1728	4.539E-4	3.65	4.01E-4	3.66
48×4	3072	1.576E-4	3.66	1.388E-4	3.5

Table 1. L^2 errors and orders of accuracy for viscous Taylor-Couette flow

with curved boundaries. The multigrid method for the fourth-order ISD method is able to achieve a speedup factor of approximately 4.

VI. Laminar flow past a cylinder

Incompressible viscous flow past a cylinder is also investigated by the SD-ACM method. We investigate two test cases with Reynolds numbers of 20 and 185 respectively based on cylinder diameter.

A 2D unstructured grid consisting of only quadrilateral elements is shown in Fig. 5. The Dirichlet boundary condition is applied for pressure and velocity at the inlet. In transverse direction, slip wall condition is employed top and bottom boundaries. Velocity values are extrapolated and pressure is fixed for outlet boundary. The cylinder wall is imposed with velocity no-slip condition where the pressure is extrapolated.

VI.A. Reynolds number 20

The predicted drag coefficient is 2.08 in our simulation which is close to the value of 2.1 measured by Tritton[27] and 2.045 computed by Dennis and Chang.[5] Figure 6 presents velocity streamlines around a cylinder at Reynolds number of 20 predicted by the fourth order SD-ACM code with a cubic wall boundary representation.

Fig. 7 presents solution convergence rates for the fourth-order ISD method on a single-p grid and a

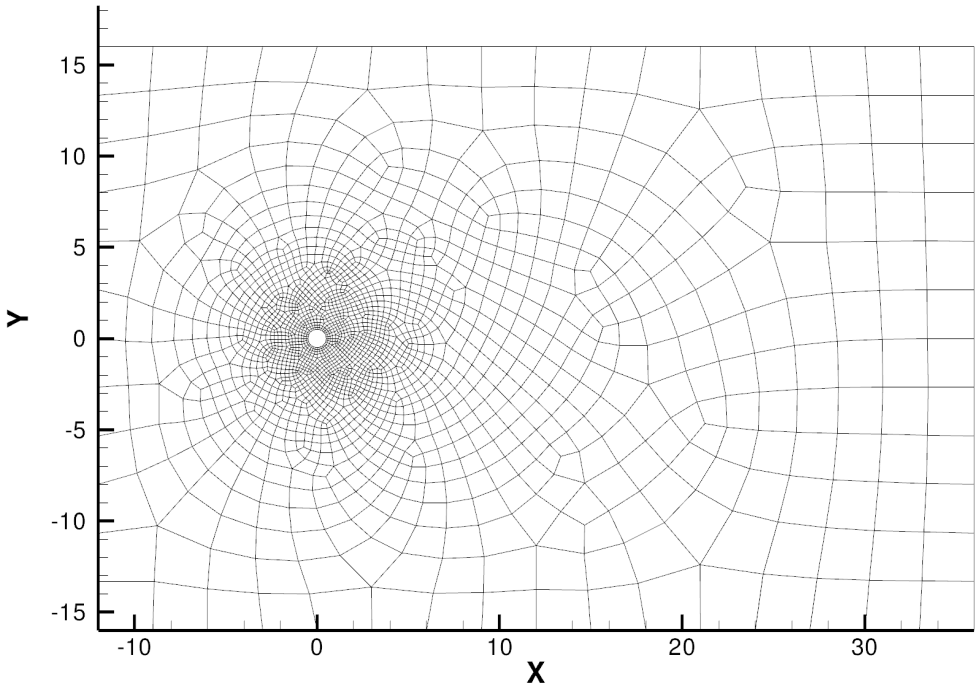

Figure 5. Computational grid for 2D flow

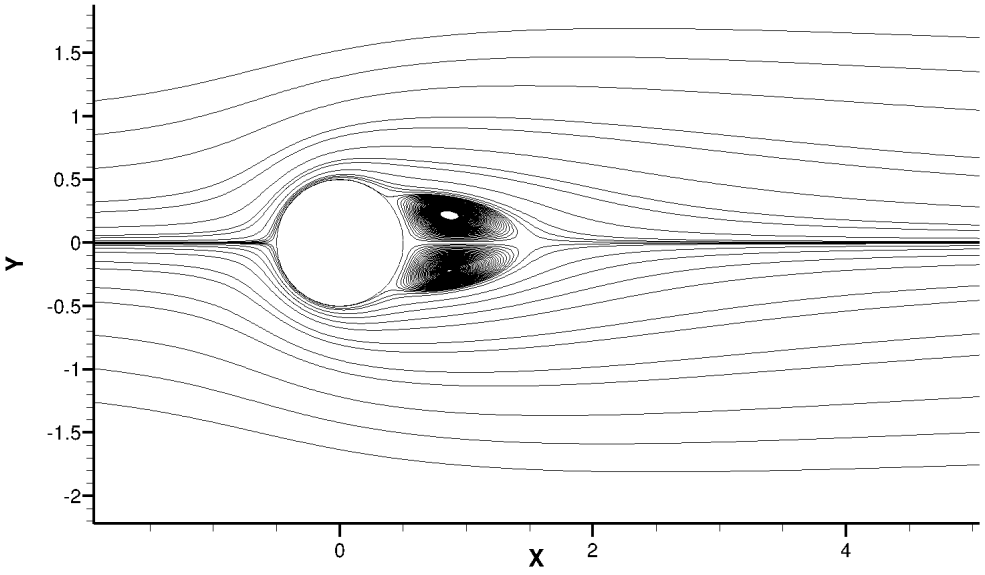

Figure 6. Velocity streamlines around a cylinder at Reynolds number 20 predicted by the fourth order ISD method

four-level p-multigrid. For the four-level p-multigrid method, we use 3 V cycles within each physical time step. Each V cycle consists of 1-1-1-6-1-1-1 times of RK5 smoothing operations at four different p levels. Fig. 7 (a) shows that the p-multigrid method is able to drop the residual to a lower level and at a faster rate. Fig. 7 (b) shows that the p-multigrid method enables a reduction of the fluctuation magnitude of the drag coefficient C_d. A possible source of the fluctuation of C_d is the transverse blockage and the relative shorter distance (12 diameters) from the center of the cylinder to the inlet.

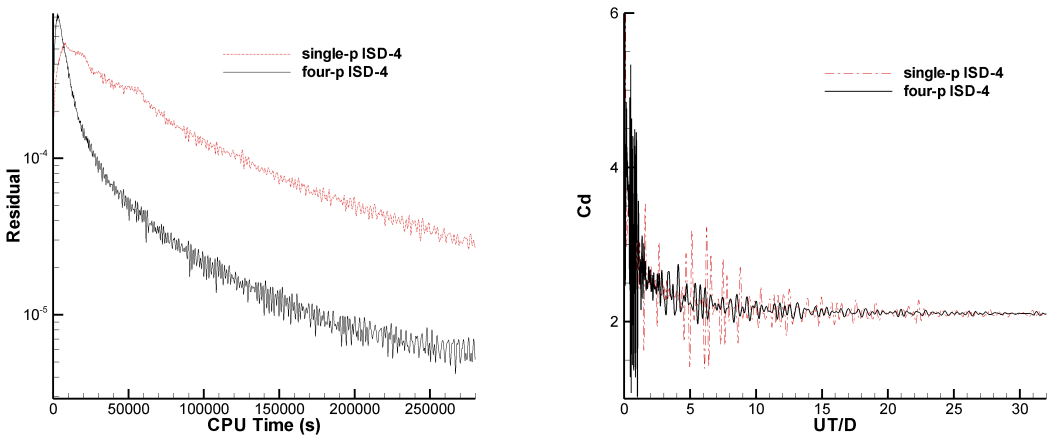

(a) Residual against CPU time (b) Cd against physical time

Figure 7. Solution convergence rates for the fourth-order ISD method on a single-p grid and a four-level p-multigrid.

VI.B. Oscillating cylinder at Reynolds number 185 on a single grid

In this section, uniform flow past a transversely oscillating cylinder is simulated at a Reynolds number of 185. The cylinder is imposed with an oscillating profile for its center with $Y(t) = A_e cos(2\pi f_e t)$. $A_e = 0.2D$ stands for the maximum amplitude of oscillation. The excitation frequency f_e is 1.1 times of the natural shedding frequency. In our simulation, the inflow velocity is 0.2m/s and the cylinder diameter is 1 meter.

We compare the time history of the lift coefficients obtained by the 2D SD-ACM code to one predicted by the PCM in Guilmineau and Queutey.[7] The agreement is excellent as shown in figure 8.

Figure 9 presents the unsteady vorticity shedding behind the oscillating cylinder at a time instant. In this simulation, the fourth-order SD method is used with the ACM and dual-time stepping approach. The cylinder wall is treated with a cubic boundary representation.[30]

VI.C. Oscillating cylinder at Reynolds number 185 on multiple grids

We again compute the unsteady flow past an oscillating cylinder at Reynolds number 185. A three-level p-multigrid method is applied. It consists of three polynomials levels, with the highest p set as 4. Within each physical time step, three V cycles are typically employed. Each V cycle consists of 1-1-6-1-1 R-K iterations at $p = 4$, $p = 2$ and $p = 1$ levels respectively. Figure 10 shows the time histories of lift and drag coefficients obtained by this three-level p-multigrid method. The ISD results agree well with the results published by Guilmineau and Queuitey.[7] Note that the ISD method with p-multigrid acceleration requires approximately one vortex shedding period to establish smooth profile of C_l and five vortex shedding periods to establish smooth time history of C_d due to initial transient period. In other words, the pressure correction method is faster to establish reasonable pressure distribution around the cylinder the ACM. Moreover, comparing to the single-level ISD method, we could achieve a speed up factor higher than 2 by this p-multigrid method for convergence of physical time marching.

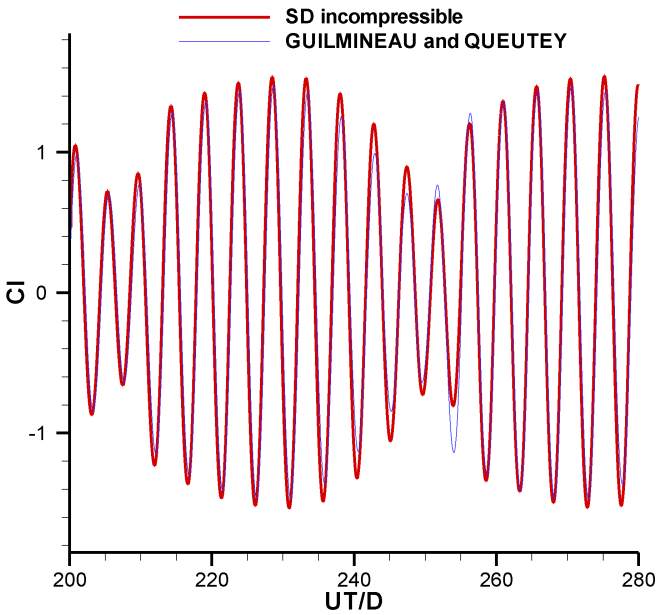

Figure 8. The lift coefficients predicted by the SD-ACM code and the PCM of Guilmineau and Queutey[7]

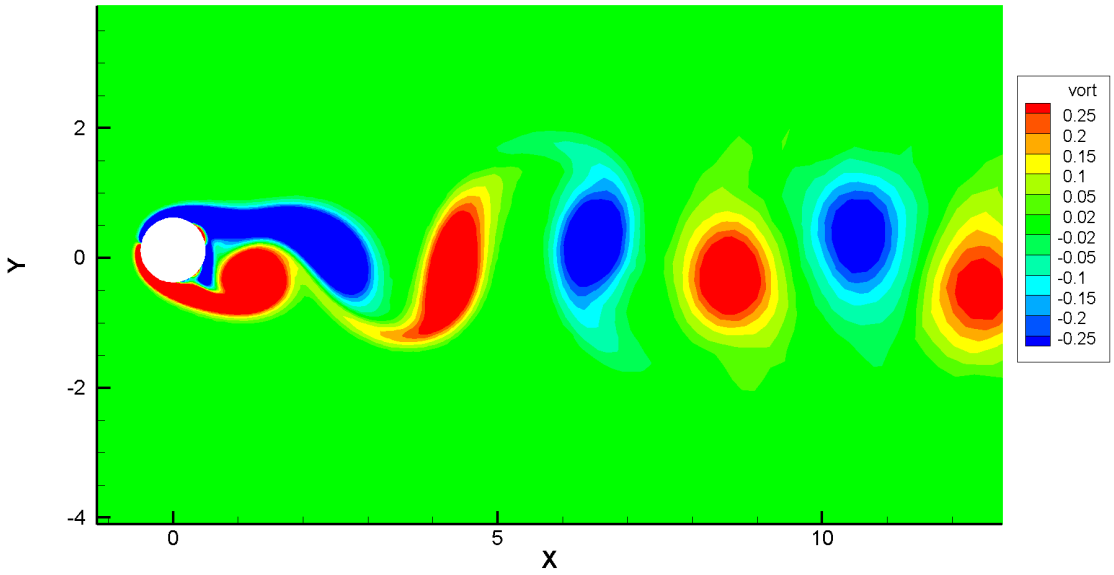

Figure 9. Velocity streamlines around a cylinder at Reynolds number 185 predicted by the fourth order SD method

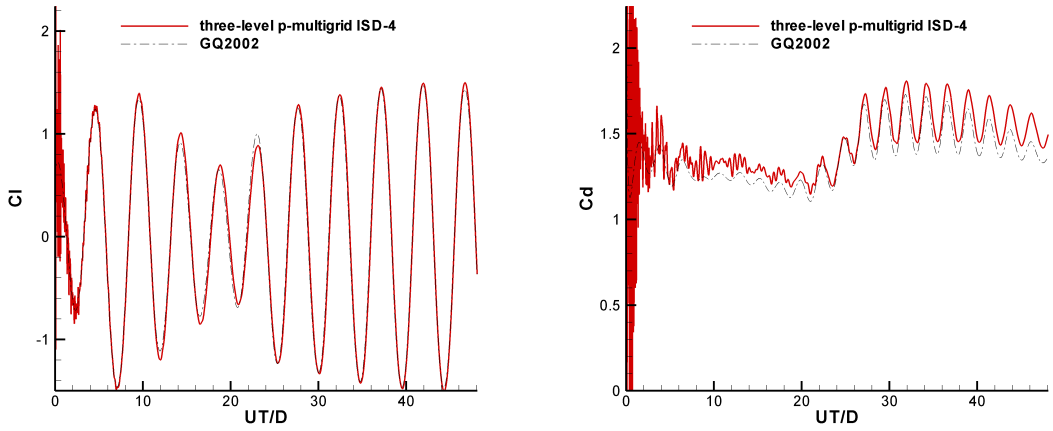

(a) Cl time history (b) Cd time history

Figure 10. Time histories of lift and drag coefficients obtained by the fourth-order ISD method on a three-level p-multigrid in comparison to the results published in Guilmineau and Queuitey.[7]

VII. Concluding Remark

An incompressible flow solver is successfully developed using the Spectral Difference method and an artificial compressibility approach. The dual time stepping technique is successfully implemented which allows this solver to solve 2D unsteady viscous flows. The ISD method is further accelerated by a p-multigrid scheme. The solvers are verified and validated using a 2D incompressible Taylor-Couette flow and a laminar flow past a circular cylinder at Reynolds number 20. Finally, this ISD solver is applied to simulate flow past an oscillating cylinder at Reynolds number 185 on a single-p-level grid as well as multiple-p-level grid. A factor of approximately four is achieved for convergence acceleration based on the present implementation for the steady viscous flow problem. A speedup factor higher than 2 is obtained for unsteady flow. The solution convergence can be further improved by an implicit time stepping method and this will be a direction of our future research. Meanwhile, the p-multigrid ACM with dual time stepping scheme can also be applied to the discontinuous Galerkin method, spectral volume method and flux reconstruction approach by Huynh,[9] etc.

VIII. Acknowledgement

Chunlei Liang would like to thank the faculty startup support from the George Washington University.

References

[1]F. Bassi and S. Rebay, High-order accurate discontinuous finite element solution of the 2D euler equations, *Journal of Computational Physics*, Vol. 138, pp. 251-285, 1997

[2]F. Bassi, A. Crivellini, D. A. Di Pietro and S. Rebay, An artificial compressibility flux for the discontinuous galerkin solution of the incompressible navier-stokes equations, *J. Comput. Phys*, Vol. 218, pp. 794-815, 2006.

[3]P. Castonguay, C. Liang and A. Jameson. Simulation of Transitional Flow over Airfoils Using the Spectral Difference Method, *AIAA Paper*, 2010-4626.

[4]A. J. Chorin, A Numerical Method for Solving Incompressible Viscous Flow Problems, *J. Comp. Phys.*, Vol. 2, pp.1226, 1967.

[5]S. C. R. Dennis and G. Chang, Numerical Solutions for Steady Flow Past a Circular Cylinder at Reynolds Numbers up to 100, *J. Fluid Mech.*, Vol. 42, pp. 471-489, 1970.

[6]J. Farmer, L. Martinelli & A. Jameson, Fast multigrid method for solving incompressible hydrodynamic problems with free surfaces, *AIAA Journal*, Vol. 32, pp. 1175-1182, 1994.

[7]E. Guilmineau and P. Queutey, A numerical simulation of vortex shedding from an oscillating circular cylinder, *Journal of Fluids and Structures*, vol 16, pp. 773-794, 2002.

[8]F. H. Harlow & J. E. Welch, Numerical Calculation of Time-Dependent Viscous Incompressible Flow with Free Surface, *Phys. Fluids*, Vol. 8, pp. 2182-2189, 1965.

[9]H.T. Huynh, A Flux Reconstruction Approach to High-Order Schemes Including Discontinuous Galerkin Methods, *AIAA paper*, AIAA-2007-4079, 2007.

[10]D. A. Kopriva, A Staggered-Grid Multidomain Spectral Method for the Compressible Navier-Stokes Equations, *Journal of Computational Physics*, Vol 143, pp. 125-158, 1998.

[11]C. Liang, K. Ou, S. Premasuthan, A. Jameson and Z. J. Wang. High-order accurate simulations of unsteady flow past plunging and pitching airfoils. *Computers and Fluids*, vol 40, pp. 236-248, 2011.

[12]C. Liang, S. Premasuthan & A. Jameson. High-order accurate simulation of flow past two side-by-side cylinders with Spectral Difference method. *Computers and Structures*, vol 87, pp. 812-817, 2009.

[13]C. Liang, A. Jameson & Z. J. Wang. Spectral Difference method for two-dimensional compressible flow on unstructured grids with mixed elements. *Journal of Computational Physics*, vol 228, pp 2847-2858, 2009.

[14]C. Liang, R. Kannan & ZJ Wang, A p-Multigrid Spectral Difference Method with explicit and implicit smoothers on unstructured triangular grids, *Computers and Fluids*, Vol. 38, pp. 254-265, 2009.

[15]C. Liang, S. Premasuthan, A. Jameson and Z. J. Wang. Large Eddy Simulation of Compressible Turbulent Channel Flow with Spectral Difference Method, *AIAA Paper*, Orlando, AIAA-2009-402.

[16]Y. Liu, M. Vinokur, & Z. J. Wang, Spectral difference method for unstructured grids I: Basic formulation, *J. of Comput. Phys.*, Vol. 216 , pp. 780-801, 2006.

[17]Y. Liu, M. Vinokur, & Z. J. Wang, Spectral (finite) volume method for conservation laws on unstructured grids V: Extension to three-dimensional systems, *Journal of Computational Physics*, Vol. 212, pp 454-472, 2006.

[18]C. Michalak & C. Ollivier-Gooch, Unstructured high-order accurate finite-volume solutions of the Navier-Stokes equations. *AIAA paper*, AIAA-2009-954.

[19]A. H. Mohammad, Z. J. Wang and C. Liang. LES of turbulent flow past a cylinder using spectral difference method. *Advances in Applied Mathematics and Mechanics*, Vol. 2, pp. 451-466, 2010.

[20]M. Parsani, G. Ghorbaniasl, C. Lacor, E. Turkel, An implicit high-order spectral difference approach for large eddy simulation, *Journal of Computational Physics*, Vol 229, pp. 5373-5393, 2010.

[21]S. Premasuthan, C. Liang, A. Jameson and Z. J. Wang, p-Multigrid Spectral Difference Method For Viscous Compressible Flow Using 2D Quadrilateral Meshes, *AIAA Paper*, AIAA-2009-950.

[22]M. Rosenfeld, D. Kwak & M. Vinokur, A Solution Method for Unsteady, Incompressible Navier-Stokes Equations in Generalized Curvilinear Coordinate Systems, *J. Comp. Phys.* Vol 94, pp. 102-137, 1991.

[23]V.V. Rusanov, Calculation of interaction of non-steady shock waves with obstacles, *Journal of Computational and Mathematical Physics USSR*, Vol. 1, pp. 267-279, 1961.

[24]R. J. Spiteri, S. J. Ruuth, A new class of optimal high-order strong-stability-preserving time discretization methods, *SIAM J. Numer. Anal.*, Vol 40, pp 469-491, 2002

[25]Y. Sun, Z. J. Wang, & Y. Liu, High-order multidomain spectral difference method for the Navier-Stokes equations on unstructured hexahedral grids, *Communication in Computational Physics*, Vol. 2, pp. 310-333, 2007.

[26]G. I. Taylor, Stability of a viscous liquid contained between two rotating cylinders, *Philos. Trans. R. Soc. London, Ser. A*, Vol. 223, pp. 289-343, 1923.

[27]D. J. Tritton, Experiments on the flow past a circular cylinder at low Reynolds numbers, *Journal of Fluid Mechanics*, Vol 6, pp. 547-567, 1959.

[28]K. Van den Abeele, C. Lacor, Z. J. Wang, On the stability and accuracy of the spectral difference method, *Journal of Scientific Computing*, vol.37, pp.162-188, 2008.

[29]Z.J. Wang, Y. Liu, G. May and A. Jameson, Spectral Difference Method for Unstructured Grids II: Extension to the Euler Equations, *Journal of Scientific Computing*, Vol. 32, pp. 45-71, 2007.

[30]Z. J. Wang & Y. Liu, Extension of the spectral volume method to high-order boundary representation, *Journal of Computational Physics*, Vol. 211, pp. 154-178, 2006.

[31]L. Yuan, Comparison of implicit multigrid schemes for three-dimensional incompressible flows, *J. Comput. Phys.*, Vol. 177, pp. 134-155, 2002.